MAP Reconstruction from Spatially Correlated PET Data

Adam Alessio, Ken Sauer, and Charles A. Bouman

***Abstract*— High sensitivity 3D PET data is often rebinned into 2D data sets in order to reduce the computation time of reconstructions. The need to precorrect the 3D data for attenuation, accidentals, scatter, and deadtime effects before rebinning along with the rebinning process itself changes the statistics of the data. This paper presents an approach for finding and using the statistics of Fourier rebinned (FORE) data. In particular, utilizing a space domain representation of FORE, we find the approximate covariance matrix of the rebinned data and model the data conditioned on the image as a low-order Markov field. This model is based on a quadratic approximation of the log-likelihood of dependent 2D PET data. The dependence relationship is then incorporated into a novel maximum *a posteriori* (MAP) 2D reconstruction method. Initial results show that this method is visually superior to traditional EM techniques and offers modest MSE improvements with a reference image over Poisson-based MAP methods.**

***Index Terms*— correlation, covariance, dependent, fully 3-D PET, Fourier Rebinning, MAP estimation, FORE**

I. Introduction

The statistical reconstruction of 3D PET data represents a formidable computational challenge. Consequently, rebinning methods, of which Fourier rebinning (FORE) [4] is the most popular, are often used to reduce the 3D data to decoupled sets of 2D data and then traditional 2D reconstruction techniques are implemented [8]. This poses a problem because these rebinning methods create 2D data which does not have the same statistics as traditional 2D data. More specifically, most statistical reconstruction techniques (all EM variations) are based on data modeled as conditionally independent Poisson variables [7], [5]. FORE rebinned data is no longer Poisson because: a) the 3D data must be fully corrected for accidentals, scatter, attenuation, and deadtime affects before applying FORE and b) the 2D data becomes a linear combination of the 3D data.

Many efforts have been made to approximate the statistics of FORE rebinned data [9], [3]. In this paper, we present a new method for more accurately modeling the rebinned 2D data as correlated variables and for reconstructing with this new model. We present a technique for finding the correlations introduced through the FORE process. Then, we reconstruct with a maximum *a posteriori* method using a quadratic approximation of the log-likelihood of this dependent data (MAP-D).

A. Alessio and K. Sauer are with the Department of Electrical Engineering, University of Notre Dame, Notre Dame, IN 46556 (e-mail: aalessio@nd.edu; sauer@nd.edu)

C. A. Bouman is with the School of Electrical Engineering, Purdue University, West Lafayette, IN 47907

II. Rationale for New Estimator

Even in idealized 3D PET systems in which the measured data closely resembles independent random variables, after FORE rebinning, the data is no longer independent. Significant improvements can be expected if one has accurate information about the correlation of the data. The following discussion presents a rough justification for incorporating correlation information into the reconstruction.

In essence, we would like to compare estimators which utilize varying amounts of correlation. In an effort to quantify the mean square error (MSE) of these estimators, we define $\mathbf{y}$ as the M dimensional rebinned sinogram, $\mathbf{x}$ as the ideal N dimensional estimated image and $\tilde{\mathbf{x}}$ as the erroneous estimated image. The linear minimum mean square error estimator would be

$$\tilde{\mathbf{x}} = E(\mathbf{x}) + \tilde{K}_{\mathbf{xy}}\tilde{K}_{\mathbf{yy}}^{-1}(\mathbf{y} - E(\mathbf{y}))$$

where $\tilde{K}_{\mathbf{xy}}$ is the erroneous $N \times M$ covariance matrix of $\mathbf{x}$ and $\mathbf{y}$. $\tilde{K}_{\mathbf{yy}}$ is the erroneous covariance function of the data in the sense that it does not include all of the correlation information. The error covariance, $\tilde{\mathbf{\Upsilon}}$, of this erroneous estimator is

$$\begin{aligned}\tilde{\mathbf{\Upsilon}} &= E[(\mathbf{x}-\tilde{\mathbf{x}})(\mathbf{x}-\tilde{\mathbf{x}})'] \\ &= K_{\mathbf{xx}} - 2\tilde{K}_{\mathbf{xy}}\tilde{K}_{\mathbf{yy}}^{-1}K_{\mathbf{yx}} + \tilde{K}_{\mathbf{xy}}\tilde{K}_{\mathbf{yy}}^{-1}K_{\mathbf{yy}}\tilde{K}_{\mathbf{yy}}^{-1}\tilde{K}_{\mathbf{yx}} \quad (1)\end{aligned}$$

where $K_{\mathbf{xx}}$ is the covariance function of $\mathbf{x}$ and $K_{\mathbf{yy}}$ is the ideal covariance function, including all of the correlation information. The error covariance of the ideal estimator is:

$$\mathbf{\Upsilon} = K_{\mathbf{xx}} - K_{\mathbf{xy}}K_{\mathbf{yy}}^{-1}K_{\mathbf{yx}} \quad (2)$$

We need to quantify how much larger $\tilde{\mathbf{\Upsilon}}$ is than $\mathbf{\Upsilon}$. Unfortunately, $K_{\mathbf{yy}}^{-1}$ would be difficult to calculate because this is no longer a diagonal matrix of independent data. Therefore, we reverted to a spectral approach. Let $K_{\mathbf{yy}} = F\Lambda_{\mathbf{yy}}F'$ be the K-L decomposition of $K_{\mathbf{yy}}$. Under an assumption of wide sense stationarity for the Poisson noise in $\mathbf{y}$ (adequate to get a rough idea of the value of the estimator), F is well approximated by the discrete Fourier transform (DFT) matrix and $\Lambda_{\mathbf{yy}}$ is a diagonal matrix containing the variances of the DFT coefficients.

Since $\mathbf{y} = \mathbf{Px} + \mathbf{n}$ where $\mathbf{n}$ is the approximately zero mean noise in the Poisson variates and $\mathbf{P}$ is the system matrix, $K_{\mathbf{xy}} = E[\mathbf{X}(\mathbf{PX}+\mathbf{N})] = \mathbf{P}E[\mathbf{XX}] + E[\mathbf{XN}]$. Assuming that the noise and the image are uncorrelated, $K_{\mathbf{xy}} = \mathbf{P}E[\mathbf{XX}]$. It also

Number of entries of K_{yy} in $\tilde{K}_{yy}$	Description of $\tilde{K}_{yy}$	$\frac{M\tilde{S}E_j}{MSE_j}$
400	When estimating y_i, includes $K_{y_a y_a}$ where $a = (i-200) \rightarrow (i+200)$	1.10
24	Includes correlation of 24 closest neighbors of y_i	1.30
8	Includes correlation of 8 closest neighbors of y_i	1.65
1	No correlation included	3.00

TABLE I

COMPARISON OF MSE VALUES FOR DIFFERENT ESTIMATORS

should be noted that $K_{\mathbf{xx}} = \tilde{K}_{\mathbf{xx}}$. When we evaluate (1) at a single pixel j,

$$M\tilde{S}E_j = k_{x_j x_j} - 2k'_{\mathbf{x}x_j}\mathbf{P}'F^*\tilde{\Lambda}_{\mathbf{yy}}^{-1}\left[2I - \Lambda_{\mathbf{yy}}\tilde{\Lambda}_{\mathbf{yy}}^{-1}\right]F^{-1}\mathbf{P}k_{\mathbf{x}x_j} \quad (3)$$

In a similar fashion, the mean square error of the ideal estimator is:

$$MSE_j = k_{x_j x_j} - k'_{\mathbf{x}x_j}\mathbf{P}'(F^*\Lambda_{\mathbf{yy}}^{-1}F^{-1})\mathbf{P}k_{\mathbf{x}x_j} \quad (4)$$

This approach simplifies the mean square error calculation to operations with diagonal matrices. The values of equations 3 and 4 were compared using a 2D covariance matrix estimated from a 70 projection x 90 angle sinogram. Table I summarizes the MSE results when differing amounts of correlation are included in $\tilde{K}_{yy}$. The last row of the table represents an estimator assuming uncorrelated data which is the current convention in the field. Consequently, with the incorporation of the correlation information of only 8 neighbors, one can expect the MSE to be approximately 55% that of the uncorrelated estimator. Once again, this assumes the the correct correlation information is known.

III. FINDING COVARIANCE

FORE essentially converts 3D sinogram data to 2D data and consists of a sum of linear operations in frequency space. This process introduces a significant amount of correlation in the data. To our knowledge, no current methods attempt to address this issue.

Using the notation of [4] and [3], with $y_{3D}()$ representing a fully 3D set of sinograms and $y_{2D}()$ representing a set of rebinned 2D sinograms, FORE can be written in the space domain as

$$y_{2D}(s,\phi,z) = \sum_{s'\phi'}\sum_{z'\Delta'} a(s-s',\phi-\phi',z,z',\Delta')y_{3D}(s',\phi',z',\Delta') \quad (5)$$

$a()$ is the FORE kernel which describes how a particular oblique plane,Δ', of plane z', affects the rebinned plane z. $a()$ can be calculated by applying FORE to 3D impulse sinograms. For instance, if $a(s,\phi,20,12,3)$ (how the 3rd oblique plane of plane 12 affects the 2D plane 20) is needed, set all oblique planes to zero and place a one at $\tilde{y}_3 D(0,0,12,3)$. Then, apply FORE to $\tilde{y}_{3D}$ and store the resulting 2D sinograms in $a(*,*,*,12,3)$.

Comtat et. al. have discussed the FORE kernel [3], but avoided using it due to computational costs. We have simplified calculation and storage issues utilizing the fact that the majority of the energy in the kernel resides near its center. We store and use only the central portion of the kernel.

FORE (5) can be written in matrix notation as

$$\mathbf{y}_{2D} = A\mathbf{y}_{3D} \quad (6)$$

where A is the matrix form of convolving by $a()$. Consequently, the covariance of the data has the form

$$K_{y_{2D}} = AK_{y_{3D}}A' \quad (7)$$

$K_{y_{3D}}$ is the covariance matrix of the 3D data. Since we assume that the 3D data is conditionally independent, this is a diagonal matrix containing only the estimated variance of the 3D data. After this transformation, the data is not independent and $K_{y_{2D}}$ is not diagonal. In fact, using a 279 projection $\times$ 360 angle sinogram from laboratory PET data, approximately 39% of the energy is not on the diagonal. The challenge now resides in how to efficiently use this covariance information.

Even with a reduced kernel size, the computation of (7) is significant. Now that we have a better understanding of the structure of true $K_{y_{2D}}$, we believe that faster methods could be used to estimate the 2D dependent covariance matrix from the 3D covariance matrix.

IV. RECONSTRUCTING WITH COVARIANCE INFORMATION

The approximate covariance matrix would make the ideal weighting matrix in reconstruction methods such as penalized, weighted least-square (PWLS) [6]. Unfortunately, this non-diagonal matrix would need to be inverted which is not feasible for reasonably sized data sets.

In our formulation, we assume that the 2D rebinned data conditioned on the image is a Markov random field. Since the exact form of the likelihood function after FORE appears intractable, we use the first and second moments to form the 2nd order Taylor series approximation of the log-likelihood.

Initially, the 3D likelihood function is Poisson and has a Taylor series approximation [2]

$$\log\mathcal{P}(\mathbf{Y}_{3D} = \mathbf{y}_{3D}|\mathbf{x}) \approx c(\mathbf{y}_{3D}) - \frac{1}{2}(\mathbf{y}_{3D} - \mathbf{P}_{3D}\mathbf{x})'\Lambda^{-1}(\mathbf{y}_{3D} - \mathbf{P}_{3D}\mathbf{x}) \quad (8)$$

where $\Lambda = \mathrm{diag}\{y_i^{-1}\}$ and is the 3D weighting matrix. It should be noted that although (8) appears to be a Gaussian likelihood, it is the second term of the Taylor series expansion of the Poisson likelihood. Please note that all of the K's and functions of K which follow are functions of y and therefore not true covariance matrices. But, all of the following algebra holds as if the Gaussian view (which uses covariance matrices)

were used. When the data is transformed to 2D through the linear operation (6), it assumes the form:

$$\log \mathcal{P}(\mathbf{Y}_{2D} = A\mathbf{y}_{3D}|\mathbf{x}) \approx c(\mathbf{y}_{2D}) \\ -\frac{1}{2}(\mathbf{y}_{2D} - \mathbf{P}_{2D}\mathbf{x})' K_{y_{2D}}^{-1}(\mathbf{y}_{2D} - \mathbf{P}_{2D}\mathbf{x}) \qquad (9)$$

$K_{y_{2D}}$ is an approximation of the 2D covariance matrix or, more accurately, the transformation of the 3D weighting matrix. As stated above, the inverse of $K_{y_{2D}}$ is not feasible, and (9) can be further simplified using a Markov assumption. That is, for a given 2D sinogram entry y_i and its neighbors $\mathbf{n}_i = \{n_1 ... n_B\}$

n_1	n_2	n_3
n_4	y_i	n_5
n_6	n_7	n_8

we need to find the distribution

$$f(y_i|\mathbf{x}, \mathbf{n}_i) = \frac{f(y_i, n_1, \ldots, n_B|\mathbf{x})}{f(n_1, \ldots, n_B|\mathbf{x})}$$

In the following, K_{fg} is the weighting for sinogram entry f and g, $\mathbf{K_{N_i}}$ is the approximate $B \times B$ weighting matrix of the neighbors,

$$\mathbf{K_{N_i}} = \begin{bmatrix} \sigma_{n_1}^2 & K_{n_1 n_2} & & \cdots & \\ K_{n_1 n_2} & \sigma_{n_2} & K_{n_2 n_3} & & \\ & \vdots & \ddots & & \\ & & & & \sigma_{n_B}^2 \end{bmatrix}$$

$$\mathbf{K_{y_i N}} = [K_{y_i n_1} K_{y_i n_2} \ldots K_{y_i n_B}]$$

$\mathbf{K_{N y_i}} = \mathbf{K_{y_i N}}'$, and $Q_i = \sigma_{y_i}^2 - \mathbf{K_{y_i N}} \mathbf{K_{N_i}^{-1}} \mathbf{K_{N y_i}}$.

Under the conditional Markov assumption, the approximation of the likelihood function simplifies to the form

$$\tilde{f}(\mathbf{y}|\mathbf{x}) \propto \\ \prod_{i=1}^{M} \exp\big(-\frac{1}{2}[(y_i - P_{i*}\mathbf{x}) - \mathbf{Z}_i(\mathbf{n_i} - \mathbf{P}_{\mathbf{n}_i *}\mathbf{x})]^2/Q_i\big) \qquad (10)$$

Where $\mathbf{Z}_i = \mathbf{K_{y_i N}} \mathbf{K_{N_i}}^{-1}$ is a $1 \times B$ vector, $P_{i*}\mathbf{x} = \sum_{k=1}^{N} P_{ik} x_k$ represents the contribution of all emission sites to projection i and $\mathbf{P}_{\mathbf{n}_i *}\mathbf{x}$ is a $B \times 1$ vector containing the contribution of emission sites to the neighbors of projection i. Q_i is a function of y which preserves the key statistical properties inherited from the Poisson likelihood of the original 3D data.

We have chosen to use a regularized estimation method in order to improve low signal-to-noise ratio cases. For all of the methods reviewed here we will use the generalized Gaussian MRF (GGMRF) model [1] , denoted as $G(x)$, as the regularization term. When this is combined with the log of (10), the overall objective function is

$$\Phi(\mathbf{x}) = G(x) + \\ \sum_{i=1}^{M} \Big[\frac{1}{2}[(y_i - P_{i*}\mathbf{x}) - \mathbf{Z}_i(\mathbf{n_i} - \mathbf{P}_{n_i *}\mathbf{x})]^2/Q_i\Big] \qquad (11)$$

The maximization of this objective function with the ICD/Newton-Raphson method found in [2] will be termed "MAP-Dependent" or MAP-D.

Algorithm	# of multi. & div.	# of matrix reads	time (sec.)
FBP	$M_0 N$	1	NA Full Recon:33.0
EM	$2M_0 N$	2	29.3
MAP-ICD	$4M_0 N$	2	30.3
MAP-D	$(2B+4)M_0 N$	2	83.7

TABLE II

COMPUTATIONAL COMPARISON OF 2D RECONSTRUCTION METHODS, LISTING APPROXIMATE MEASURES OF COMPUTATIONAL TIME PER FULL ITERATION. M_0 IS THE NUMBER OF NONZERO PROJECTIONS ASSOCIATED WITH EACH OF THE N PIXELS. FOR THE TIME STUDY, MAP-D USED $B = 8$

V. IMPLEMENTATION AND RESULTS

The MAP-D method consists of the following steps:

1. Generate FORE kernels for a particular 3D data size
2. Collect data in fully 3D mode
3. If desired, correct 3D data for attenuation, deadtime, detector efficiencies, decay
4. Estimate 3D weighting matrix and transform into 2D with FORE kernels (7)
5. FORE rebin data [4]
6. Minimize dependent objective function(11)

Along with improving the quality of the reconstruction from rebinned data, another primary goal of this estimator is to provide a faster alternative to fully 3D reconstruction. Table II compares the computational load of the proposed MAP-D algorithm with other two dimensional reconstruction algorithms. The time column presents the average time for one iteration of a 128×128 image using a 279×360 data set on a Sun Blade1000 Workstation with 512Mb of RAM. P is a sparse matrix containing $M_0 N$ nonzero entries. MAP-D requires a $2BM_0N$ more multiplies than traditional MAP-ICD due to the matrix multiplications necessary in the optimization. This may seem exceptionally slow, but the multiplications do not dominate the computation time during each iteration as shown in the similar times for EM and MAP-ICD and in the fact that MAP-D has $16\times$ the multiplications as MAP-ICD, but only requires $3\times$ the time.

Even though the computation per iteration is reasonable, the setup time for MAP-D is significant and remains an area for improvement. MAP-D requires two significant steps before beginning to optimize the objective. First of all, the transformation of the 3D weighting to 2D is currently a non-optimal $O(M^2 K_s^2 Z_{pl}^2)$ process where M is the size of the sinogram, K_s is the size of one dimension of the FORE kernel, and Z_{pl} is the number of detector planes. Secondly, MAP-D must also compute Z_i for all M projections which involves M $B \times B$ matrix inversions (for a total complexity of $O(M * B^3)$). Even with these steps, MAP-D remains substantially faster than fully 3D algorithms.

Testing has revealed that the MAP-D method is visually comparable to the traditional Poisson model MAP. It also offers slight improvements in the MSE error between the true image and the reconstructions. For all trials, we included only 8 neighbors of y_i ($B = 8$). Initially, we compared reconstructions of

simulated 3D Shepp phantoms. These were forward projected into 180 $\times$ 150 sinograms and Poisson noise and uniform scatter were introduced. With the same prior influence, the MAP-D reconstruction had 80% of the MSE of the original MAP reconstruction.

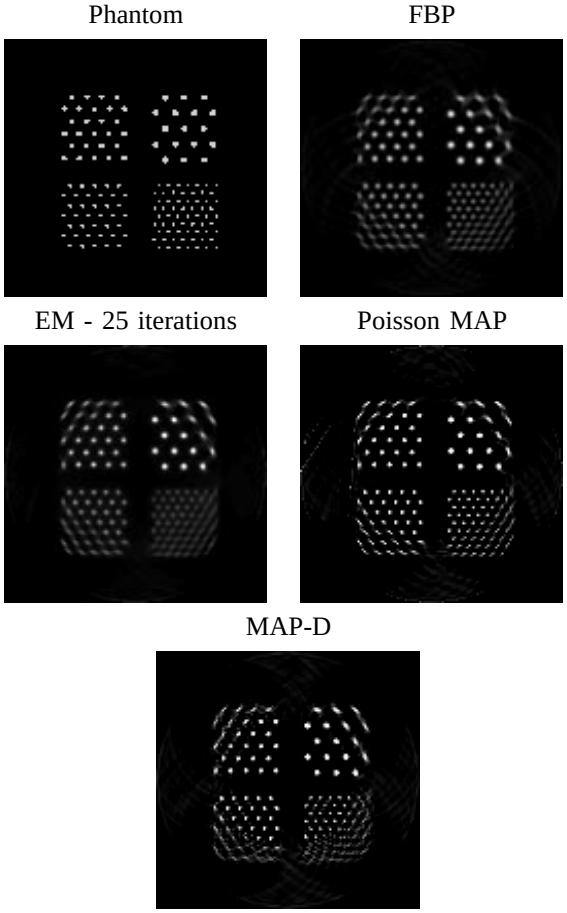

Fig. 1. 128x128 Reconstructions of Simulated Derenzo-like phantom from FORE rebinned 279x360 data. Consists of 4 quadrants with 5.6 mm diameter hot spots to 2.8 mm hot spots.

Figure 1 shows reconstructions from a simulated 3D Derenzo-like phantom. This phantom spanned 7 planes of a 24 ring scanner and was 3D forward projected to 279 $\times$ 360 sinograms. Poisson noise and 20% uniform scatter were added. No other physical effects (attenuation, deadtime, etc.) were incorporated. For the MAP-D method, the approximate 2D covariance matrix was computed from the 3D data through the use of 30 $\times$ 30 FORE kernels. For all reconstructions, the sinograms were FORE rebinned into 47 2D planes. The filtered backprojection reconstruction used an 80% cutoff Hanning filter. MAP and MAP-D required 10 iterations to reach close to convergence. Once again, the MAP-D method is visually similar to the traditional Poisson model MAP. Figure 2 reveals the central portion from these reconstructions along a vertical line, and shows that the MAP-D and MAP methods are equally

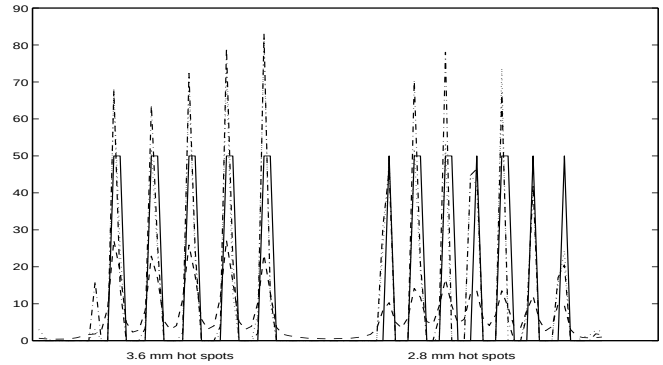

Fig. 2. Central portion of horizontal line 73 from simulated phantom. Reference image (solid), EM (dashed), Poisson MAP (dashdot), MAP-D (dotted)

capable of resolving the lower right, 2.8 mm hot spots (the EM and FBP approaches are not).

For this simulated phantom, MAP-D yields recons with 95% the MSE of MAP. This value, along with the 80% from the Shepp trials, are not as positive as the 55% expected from table I. Given that this expected figure is based on a stationarity assumption and approximate covariance taken from the center of the sinogram, some discrepancy is to be expected.

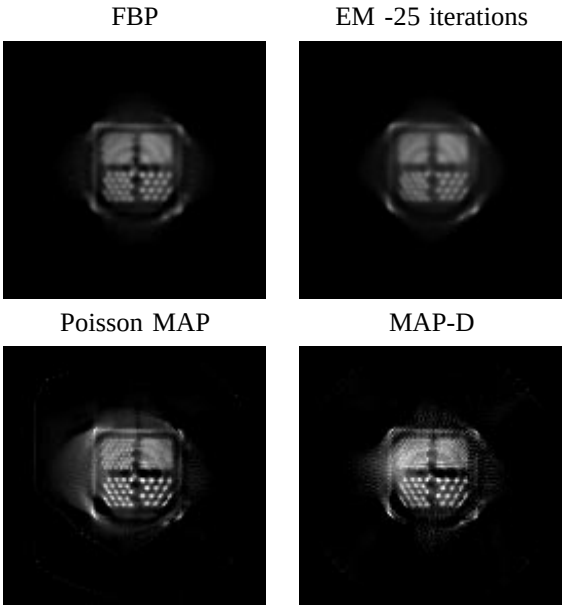

Fig. 3. 128x128 Reconstructions of Real Derenzo-like phantom from FORE rebinned 279x360 data. Consists of 4 quadrants with 4.0 mm diameter hot spots to 1.6 mm hot spots.

The method was also tested with clinical data from the IndyPET-II scanner [11] on a phantom similar to the simulated version. 6.9×10^8 events were collected in fully 3D mode and stored in 216 oblique 279 $\times$ 360 sinograms. No corrections were applied to the data which was FORE rebinned into 47 direct sinograms. Figure 3 displays reconstructions of this data.

Although the degradation due to printing may not reveal this, there exists a clear variance in contrast across the image and methods such as those in [10] may aid in compensating for the spatially variant 3D detector response.

VI. Conclusions

Theoretically, the introduction of correlation information should enhance reconstructions. Modest gains in terms of MSE with a reference image have been presented. Current visual results do not strongly support the use of MAP-D. Several stages of this approach need improvement. For instance, we need to improve the choice of 3D weighting matrices especially with corrected 3D data. Moreover, we hope to speed and refine the transformation of the 3D weighting matrix to the 2D domain. The quadratic approximation of the 3D likelihood may need to be changed to enhance visual results. Most importantly, further testing may reveal that the inclusion of more neighbors is necessary in order to yield higher quality reconstructions. The introduction of more neighbors will increase reconstruction time leading to the need for faster optimization methods.

VII. Acknowledgments

This work was supported by a grant from the State of Indiana 21st Century Research and Technology Fund. We thank Ned Rouze and Gary Hutchins of Indiana University for the use of data from the IndyPET-II scanner.

References

[1] C. A. Bouman and K. Sauer. A generalized Gaussian image model for edge-preserving map estimation. *IEEE Trans. on Image Processing*, 2:296–310, July 1993.

[2] C. A. Bouman and K. Sauer. A unified approach to statistical tomography using coordinate descent optimization. *IEEE Trans. on Image Processing*, 5(3):480–492, March 1996.

[3] C. Comtat, P. Kinahan, M. Defrise, C. Michel, and D. Townsend. Fast reconstruction of 3D PET data with accurate statistical modeling. *IEEE Trans. on Nuclear Science*, 45(3):1083–1089, June 1998.

[4] M. Defrise, P.E. Kinahan, D.W. Townsend, C. Michel, M. Sibomana, and D.F. Newport. Exact and approximate rebinning algorithms for 3-D PET data. *IEEE Trans. on Medical Imaging*, 16(2):145–158, 1997.

[5] J. Fessler and A. Hero. Penalized maximum-likelihood image reconstruction using space-alternating generalized EM algorithms. *IEEE Trans. on Image Processing*, 4(10):1417–1429, October 1995.

[6] J.A. Fessler. Penalized weighted least-squares image reconstruction for positron emission tomography. *IEEE Trans. on Medical Imaging*, 13(2):290–299, June 1994.

[7] H.M. Hudson and R.S. Larkin. Accelerated image reconstruction using ordered subsets of projection data. *IEEE Trans. on Medical Imaging*, 13(4):601–609, December 1994.

[8] M. Krzywinski, V. Sossi, and T.J. Ruth. Comparison of FORE, OSEM, and SAGE algorithms to 3DRP in 3D PET using phantom and human subject data. *IEEE Trans. on Nuclear Science*, 46(4):1114–1120, 1999.

[9] X. Liu, C. Comtat, C. Michel, P. Kinahan, M. Defrise, and D. Townsend. Comparison of 3-D reconstruction with 3D-OSEM and with FORE+OSEM for PET. *IEEE Trans. on Medical Imaging*, 20(8):804–814, August 2001.

[10] J. Qi and R.M. Leahy. Resolution and noise properties of MAP recon for fully 3D PET. *IEEE Trans. on Medical Imaging*, 19(5):493–506, May 2000.

[11] N. Rouze, K. Stantz, and G. Hutchins. Design of IndyPET-II, high-resolution, high-sensitivity research scanner. In *Proc. of IEEE Nucl. Sci. Symp. and Med. Imaging Conf.*, San Diego, CA, 2001.